

Orbital magnetization and its effect in antiferromagnets on the distorted fcc lattice

Zhigang Wang and Ping Zhang*

*Institute of Applied Physics and Computational Mathematics,
P.O. Box 8009, Beijing 100088, P.R. China*

Junren Shi

Institute of Physics, P.O. Box 603, CAS, Beijing 100080, P.R. China

Abstract

We study the intrinsic orbital magnetization (OM) in antiferromagnets on the distorted face-centered-cubic lattice. The combined lattice distortion and spin frustration induce nontrivial k -space Chern invariant, which turns to result in profound effects on the OM properties. We derive a specific relation between the OM and the Hall conductivity, according to which it is found that the intrinsic OM vanishes when the electron chemical potential lies in the Mott gap. The distinct behavior of the intrinsic OM in the metallic and insulating regions is shown. The Berry phase effects on the thermoelectric transport is also discussed.

PACS numbers: 72.15.Jf, 75.20.-g, 75.47.-m

*Corresponding author. Electronic address: zhang_ping@iapcm.ac.cn

I. INTRODUCTION

The orbital magnetism of Bloch electrons has been an outstanding problem in solid state physics, and attracted renewed interest due to the recent recognition [1, 2, 3] that the Berry phase effect plays a very important role in the orbital magnetism. The issue was carried out in the powerful semiclassical formalism [4, 5], in which the Bloch electron for n -th band is treated as a wave packet $|w_n(\mathbf{r}_c, \mathbf{k}_c)\rangle$ with its center $(\mathbf{r}_c, \mathbf{k}_c)$ in the phase space. The orbital magnetic moment characterizes the rotation of the wave packet around its centroid and is given by $\mathbf{m}_n(\mathbf{k}_c) = \frac{(-e)}{2} \langle w_n | (\hat{\mathbf{r}} - \mathbf{r}_c) \times \hat{\mathbf{v}} | w_n \rangle$, where $(-e)$ is the charge of the electron and $\hat{\mathbf{v}}$ is the velocity operator. By writing the wave packet in terms of the Bloch state, one obtains (\mathbf{k}_c is abbreviated as \mathbf{k})

$$\mathbf{m}_n(\mathbf{k}) = -i(e/2\hbar) \langle \nabla_{\mathbf{k}} u_{n\mathbf{k}} | \times [\hat{H}_{\mathbf{k}} - \varepsilon_{n\mathbf{k}}^{(0)}] | \nabla_{\mathbf{k}} u_{n\mathbf{k}} \rangle, \quad (1)$$

where $|u_{n\mathbf{k}}\rangle$ is the periodic part of the Bloch state with band energy $\varepsilon_{n\mathbf{k}}^{(0)}$, and $\hat{H}_{\mathbf{k}}$ is the crystal Hamiltonian acting on $|u_{n\mathbf{k}}\rangle$. Equation (1) can be alternatively derived by taking the differential of the electron energy, which within first order in the perturbative magnetic field \mathbf{B} turns to be $\varepsilon_{n\mathbf{k}} = \varepsilon_{n\mathbf{k}}^{(0)} - \mathbf{m}_n(\mathbf{k}) \cdot \mathbf{B}$, with respect to \mathbf{B} . It was further found [1] that the presence of a weak magnetic field \mathbf{B} will result in a modification of the density of states in the semiclassical phase space, $d^3\mathbf{k} \rightarrow d^3\mathbf{k}(1 + e\mathbf{B} \cdot \boldsymbol{\Omega}_n/\hbar)$, where $\boldsymbol{\Omega}_n(\mathbf{k}) = i \langle \nabla_{\mathbf{k}} u_{n\mathbf{k}} | \times | \nabla_{\mathbf{k}} u_{n\mathbf{k}} \rangle$ is the Berry curvature in k -space. Due to this weak-field modification, a quantum-state summation $\sum_{\mathbf{k}} \mathcal{O}(\mathbf{k})$ of some physical quantity $\mathcal{O}(\mathbf{k})$ should be converted to an integral according to $\int d^3\mathbf{k}(1 + e\mathbf{B} \cdot \boldsymbol{\Omega}_n/\hbar) \mathcal{O}(\mathbf{k})$. Additional thermodynamic average over Bloch bands should be included at finite temperature. Therefore, the total free energy for an equilibrium ensemble of electrons in the weak field may be written as

$$F = -\frac{1}{\beta} \sum_n \int d^3\mathbf{k} \left(1 + \frac{e}{\hbar} \mathbf{B} \cdot \boldsymbol{\Omega}_n(\mathbf{k}) \right) \ln[1 + e^{\beta(\mu - \varepsilon_{n\mathbf{k}})}]. \quad (2)$$

where μ is the electron chemical potential and $\beta = 1/k_B T$. The equilibrium orbital magnetization (OM) density is given by the field derivative at fixed temperature and chemical

potential, $\vec{\mathcal{M}} = -(\partial F/\partial \mathbf{B})_{\mu,T}$, with the result

$$\begin{aligned}\vec{\mathcal{M}} &= \sum_n \int d^3\mathbf{k} \mathbf{m}_n(\mathbf{k}) f_n \\ &+ \frac{1}{\beta} \sum_n \int d^3\mathbf{k} \frac{e}{\hbar} \boldsymbol{\Omega}_n(\mathbf{k}) \ln [1 + e^{\beta(\mu - \varepsilon_{n\mathbf{k}})}] \\ &\equiv \mathbf{M}_c + \mathbf{M}_\Omega,\end{aligned}\tag{3}$$

where f_n is the local equilibrium Fermi function for n -th band. In addition to the conventional term \mathbf{M}_c in terms of the orbital magnetic moment $\mathbf{m}_n(\mathbf{k})$, the extra term \mathbf{M}_Ω in Eq. (3) is a Berry phase effect and exposes a new topological ingredient to the orbital magnetism. Interestingly, it is this Berry phase correction that eventually enters the thermal transport current [3]. At zero temperature and magnetic field the general expression (3) is reduced to

$$\vec{\mathcal{M}} = \sum_n \int^{mu_0} d^3\mathbf{k} \left(\mathbf{m}_n(\mathbf{k}) + \frac{e}{\hbar} \boldsymbol{\Omega}_n(\mathbf{k}) [\mu_0 - \varepsilon_{n\mathbf{k}}] \right),\tag{4}$$

where the upper limit means that the integral is over states with energies below the zero-temperature chemical potential (Fermi energy) μ_0 .

The Berry phase effect on orbital magnetism was until now partially presented by very few studies. Recent observation of the anomalous Nernst effect (ANE) in $\text{CuCr}_2\text{Se}_{4-x}\text{Br}_x$ compound [6] was attributed [3] to the manifestation of the Berry phase effect in the OM. Also the orbital magnetism was recently studied by use of two-dimensional (2D) Haldane model and ferromagnetic *kagomé* lattice with spin chirality [7, 8]. These two models are rare examples to show the zero-field quantum Hall effect (QHE) [9, 10]. From Ref. [8] one learns that the Berry phase effect causes the OM to display different behavior in metallic and insulating regions. This difference may be explained in parallel with Haldane's recent finding [11] of the Berry phase effect in the intrinsic Hall conductivity [including QHE and anomalous Hall effect (AHE)].

The objective of the present paper is dual. First we remark that the Berry phase effect on the orbital magnetism has been included in the well-known Kubo-Streda formula [12]. Therefore, a full quantum-mechanical linear response theory of the OM can be developed as a useful complement of the semiclassical formalism, although the latter looks more elegant and practical for calculation on clean samples. Then we examine the 3D problem by studying the orbital magnetism in antiferromagnets on the distorted face-centered-cubic (fcc) lattice. The

results reveal that a general “*topological orbital magnetism theory*” that takes into account Berry phase effect must now be developed.

The paper is organized as follows. In the next section, we address that the intrinsic OM given in the semiclassical formalism is consistent with the well-known quantum-mechanical Kubo-Streda formula in the clean-sample limit. Section III describes the physical model that is used in this work. The topological property and the consequent intrinsic Hall effect associated with the model are also given in this section. In Sec. IV, we present a detailed study of the properties of the OM and its effects on transport response in antiferromagnets on the distorted fcc lattice. Finally, in Sec. V we present our conclusions.

II. KUBO-STREDA FORMULA OF THE ORBITAL MAGNETIZATION

Due to the above mentioned modification of the density of states, the particle number in the weak magnetic field (say, along z -axis) is given by

$$N(B, \mu) = \sum_n \int d^3\mathbf{k} \left(1 + \frac{e}{\hbar} B \Omega_n^z(\mathbf{k}) \right) f_n. \quad (5)$$

It is easy to see that a link between Eq. (3) and Eq. (5) is $\left(\frac{\partial \mathcal{M}_z}{\partial \mu} \right)_B = \left(\frac{\partial N}{\partial B} \right)_\mu$, which is nothing but the usual thermodynamic Maxwell relation and therefore should be free from the weak-field limit used by the semiclassical approach. Thus the zero-field OM is given by

$$\mathcal{M}_z = \lim_{B \rightarrow 0} \int^\mu \left(\frac{\partial N(B, \mu')}{\partial B} \right)_{\mu'} d\mu'. \quad (6)$$

On the other side, the integrand in Eq. (6) can be written in terms of Kubo-Streda [12] formula for electrons as follows

$$\sigma_{xy}|_\mu = \sigma_{xy}^I|_\mu - e \frac{\partial N(B, \mu)}{\partial B}, \quad (7)$$

where $\sigma_{xy}|_\mu$ is the Hall conductivity and

$$\sigma_{xy}^I|_\mu = i \frac{e^2 \hbar}{2} \int d\epsilon \frac{\partial f(\epsilon, \mu)}{\partial \epsilon} \text{Tr}[\hat{v}_x G^+(\epsilon) \hat{v}_y \delta(\epsilon - \hat{H}) - \hat{v}_x \delta(\epsilon - \hat{H}) \hat{v}_y G^-(\epsilon)]. \quad (8)$$

Here $G^\pm(\mu) = \lim_{\eta \rightarrow 0^+} (\mu - \hat{H} \pm i\eta)^{-1}$ is the operator Green function and \hat{v}_α is the velocity operator. In Bloch-state representation the trace in Eq. (6) is equivalent to $\sum_{n\mathbf{k}} \langle u_{n\mathbf{k}} | (\dots) | u_{n\mathbf{k}} \rangle$ with the Hamiltonian transformed to $\hat{H}_{\mathbf{k}} = e^{i\mathbf{k} \cdot \mathbf{r}} \hat{H} e^{-i\mathbf{k} \cdot \mathbf{r}}$ and the velocity to $\hat{v}_\alpha(\mathbf{k}) = \frac{1}{\hbar} \frac{\partial \hat{H}_{\mathbf{k}}}{\partial k_\alpha}$.

Replacing $\frac{\partial f(\epsilon, \mu)}{\partial \epsilon}$ in Eq. (8) by $-\frac{\partial f(\epsilon, \mu)}{\partial \mu}$ and using the completeness relation of the Bloch states, $\sum_{n\mathbf{k}} |u_{n\mathbf{k}}\rangle \langle u_{n\mathbf{k}}| = 1$, one has

$$\begin{aligned} \int^\mu \sigma_{xy}^I |_{\mu'} d\mu' &= -i \frac{e^2 \hbar}{2} \lim_{\eta \rightarrow 0^+} \int d\epsilon f(\epsilon, \mu) \times \sum_{\substack{n, \mathbf{k} \\ n', \mathbf{k}'}} \left\{ \frac{\delta(\epsilon - \epsilon_{n\mathbf{k}})}{\epsilon - \epsilon_{n'\mathbf{k}'} + i\eta} \langle u_{n\mathbf{k}} | \hat{v}_x(\mathbf{k}) | u_{n'\mathbf{k}'} \rangle \langle u_{n'\mathbf{k}'} | \hat{v}_y(\mathbf{k}) | u_{n\mathbf{k}} \rangle \right. \\ &\quad \left. - \frac{\delta(\epsilon - \epsilon_{n\mathbf{k}})}{\epsilon - \epsilon_{n'\mathbf{k}'} - i\eta} \langle u_{n\mathbf{k}} | \hat{v}_y(\mathbf{k}) | u_{n'\mathbf{k}'} \rangle \langle u_{n'\mathbf{k}'} | \hat{v}_x(\mathbf{k}) | u_{n\mathbf{k}} \rangle \right\} \\ &= \frac{e^2}{\hbar} \sum_{\substack{n, \mathbf{k} \\ n', \mathbf{k}'}} f(\epsilon_{n\mathbf{k}}, \mu) \frac{\text{Im} \left\{ \langle u_{n\mathbf{k}} | \frac{\partial \hat{H}_{\mathbf{k}}}{\partial k_x} | u_{n'\mathbf{k}'} \rangle \langle u_{n'\mathbf{k}'} | \frac{\partial \hat{H}_{\mathbf{k}}}{\partial k_y} | u_{n\mathbf{k}} \rangle \right\}}{\epsilon_{n\mathbf{k}} - \epsilon_{n'\mathbf{k}'}}. \end{aligned} \quad (9)$$

By use of the identity

$$\frac{\partial \hat{H}_{\mathbf{k}}}{\partial k_\alpha} |u_{n\mathbf{k}}\rangle = \frac{\partial \epsilon_{n\mathbf{k}}}{\partial k_\alpha} |u_{n\mathbf{k}}\rangle + (\epsilon_{n\mathbf{k}} - \hat{H}_{\mathbf{k}}) \left| \frac{\partial u_{n\mathbf{k}}}{\partial k_\alpha} \right\rangle \quad (10)$$

and after a transformation of \mathbf{k} -sum to an integral, Eq. (9) is ready to be simplified as

$$\int^\mu \sigma_{xy}^I |_{\mu'} d\mu' = \frac{e^2}{\hbar} \sum_n \int d^3 \mathbf{k} f_n \text{Im} \left\{ \left\langle \frac{\partial u_{n\mathbf{k}}}{\partial k_x} \left| \hat{H}_{\mathbf{k}} - \epsilon_{n\mathbf{k}} \right| \frac{\partial u_{n\mathbf{k}}}{\partial k_y} \right\rangle \right\}. \quad (11)$$

A comparison of Eq. (11) with Eq. (1) immediately gives the following relation

$$\begin{aligned} \int^\mu \sigma_{xy}^I |_{\mu'} d\mu' &= e \sum_n \int d^3 \mathbf{k} m_n^z(\mathbf{k}) f_n \\ &= e M_c^{(z)}, \end{aligned} \quad (12)$$

where the second line is obtained by using the definition of \mathbf{M}_c in Eq. (3). Thus one finds that the semiclassical expression for \mathbf{M}_c is equivalent to the quantum-mechanical expression for $(1/e) \int^\mu \sigma_{xy}^I |_{\mu'} d\mu'$. Note that although σ_{xy}^I is a Fermi-surface term, the quantity $\int^\mu \sigma_{xy}^I |_{\mu'} d\mu'$ is a Fermi-sea term and all the Bloch states below μ should be accounted when calculating the OM. On the other side, in the clean limit, the Kubo formula for the Hall conductivity $\sigma_{xy} |_{\mu}$ can be written in terms of the Berry curvatures Ω_n^z [13],

$$\sigma_{xy} |_{\mu} = -\frac{e^2}{\hbar} \sum_n \int d^3 \mathbf{k} f_n \Omega_n^z. \quad (13)$$

From Eq. (13) one has

$$\int^\mu \sigma_{xy} |_{\mu'} d\mu' = -\frac{1}{\beta} \frac{e^2}{\hbar} \sum_n \int d^3 \mathbf{k} \Omega_n(\mathbf{k}) \ln [1 + e^{\beta(\mu - \epsilon_{n\mathbf{k}})}], \quad (14)$$

which is exactly the semiclassical expression for the Berry phase term $eM_{\Omega}^{(z)}$ in Eq. (3). Thus the semiclassical OM in Eq. (3) can actually be written as a Kubo-Streda formula:

$$\mathcal{M}_z = \frac{1}{e} \int^{\mu} \sigma_{xy}^I|_{\mu'} d\mu' - \frac{1}{e} \int^{\mu} \sigma_{xy}|_{\mu'} d\mu'. \quad (15)$$

The other two components \mathcal{M}^x and \mathcal{M}^y are given in a similar manner. This equivalence between the semiclassical and quantum-mechanical description for the OM is only valid in the intrinsic region and will break down when the impurity scattering effect is included. Thus while the semiclassical formula of the OM is more suitably employed to study the intrinsic property of the OM, the Kubo-Streda formula must be used when one takes into account the impurity scattering. Another aspect is that the Kubo-Streda formula is valid in arbitrary strength of the external magnetic field, while the semiclassical formula only works in the weak field limit. In some special cases, for example, when one wants to know the edge state effect on the OM in a finite-size sample in a strong magnetic field B [14, 15], a more apparent approach can be employed by directly calculating the total free energy and then a finite-field OM is obtained by a B -derivative of the free energy.

III. SPECIFIC MODEL AND 2D CHERN NUMBER

Now we focus our attention to the properties of the OM in a specific spin-frustrated system. As in Ref. [16], the model we used describes the chiral spin state in the ordered antiferromagnet (AF) on the three-dimensional fcc lattice. The AF on the fcc lattice is a typical frustrated system, and nontrivial triple- Q spin structure with finite spin chirality has been revealed by band structure calculation [17] and observed in experiments [18, 19]. The anomalous behaviors in the fcc AF were also observed. For example, there occurs mysterious weak ferromagnetism in NiS_2 below the second AF transition temperature [20]. The Hall conductivity in this material is also large and strongly temperature dependent [21]. In $\text{Co}(\text{S}_x\text{Se}_{1-x})_2$, the AHE is enhanced in the intermediate x region, where the nontrivial magnetism is realized [22].

The triple- Q spin structure on fcc lattice is shown in Fig. 1. Here the lattice points are divided into four sublattices with different local spins \vec{S}_a ($a = 1, 2, 3, 4$) on them. The AF nature requires $\sum_a \vec{S}_a = 0$. The minimization of the 2-spin exchange interaction energy cannot uniquely determine the sublattice spin orientation. The inclusion of higher order

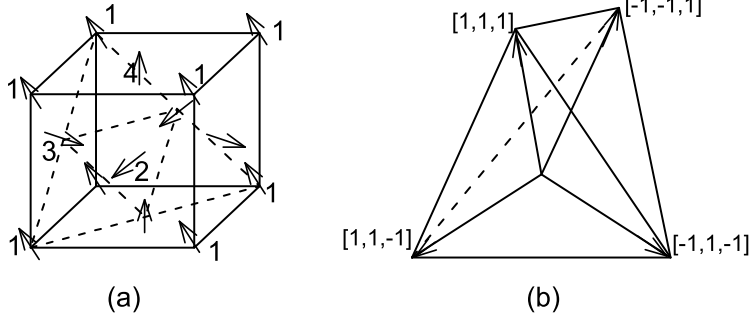


FIG. 1: (a) Triple- Q spin structure on fcc lattice. (b) Relation of the 4-spin moments \vec{S}_a ($a = 1, 2, 3, 4$).

(4-spin exchange) interaction $H_4 = J_4 \sum_{a \neq b} (\vec{S}_a \cdot \vec{S}_b)^2$ with positive J_4 gives the ground-state spin configuration [23, 24] as $\vec{S}_1 = (\frac{1}{\sqrt{3}}, \frac{1}{\sqrt{3}}, \frac{1}{\sqrt{3}})$, $\vec{S}_2 = (\frac{1}{\sqrt{3}}, -\frac{1}{\sqrt{3}}, -\frac{1}{\sqrt{3}})$, $\vec{S}_3 = (-\frac{1}{\sqrt{3}}, \frac{1}{\sqrt{3}}, -\frac{1}{\sqrt{3}})$, and $\vec{S}_4 = (-\frac{1}{\sqrt{3}}, -\frac{1}{\sqrt{3}}, \frac{1}{\sqrt{3}})$, where each direction corresponds to the four corners from the center of a tetrahedron [Fig. 1(b)]. The effective Hamiltonian for the hopping electrons strongly coupled to the mean-field effective magnetic field caused by these local spins is given by $H = \sum_{NN} t_{ij}^{eff} \psi_i^\dagger \psi_j$ with $t_{ij}^{eff} = t \langle \chi_i | \chi_j \rangle = t e^{ia_{ij}} \cos \frac{\vartheta_{ij}}{2}$. Here the spin wave function $|\chi_i\rangle$ is explicitly given by $|\chi_i\rangle = [\cos \frac{\vartheta_i}{2}, e^{i\phi_i} \sin \frac{\vartheta_i}{2}]^T$, where the polar coordinates are pinned by the local spins, i.e., $\langle \chi_i | \vec{S}_i | \chi_i \rangle = \frac{1}{2} (\sin \vartheta_i \cos \phi_i, \sin \vartheta_i \sin \phi_i, \cos \vartheta_i)$. ϑ_{ij} is the angle between the two spins \vec{S}_i and \vec{S}_j . The phase factor a_{ij} can be regarded as the gauge vector potential $a_\mu(\mathbf{r})$, and the corresponding gauge flux is related to scalar spin chirality $\chi_{ijk} = \vec{S}_i \cdot (\vec{S}_j \times \vec{S}_k)$ [25]. In periodic crystal lattices, the non-vanishing of the gauge flux relies on the multiband structure with each band being characterized by a Chern number. The Chern number appears as a result of the spin-orbit interaction and/or spin chirality in ferromagnets. In ferromagnets the time-reversal broken symmetry is manifest, while in AF the time-reversal operation combined with the translation operation often constitutes the unbroken symmetry. In the latter case, the nonzero Hall conductivity σ_{xy} is forbidden. However, when there are more than two sublattices and the spin structure is noncollinear, this combined symmetry would be absent and finite σ_{xy} is not forbidden [16].

The net spin chirality for the ideal fcc AF lattice in Fig. 1 is zero, because the spin chiralities are the vector quantities and the sum of these four vectors is zero. However, when the lattice is distorted along the $[1,1,1]$ direction, then the non-zero net spin chirality

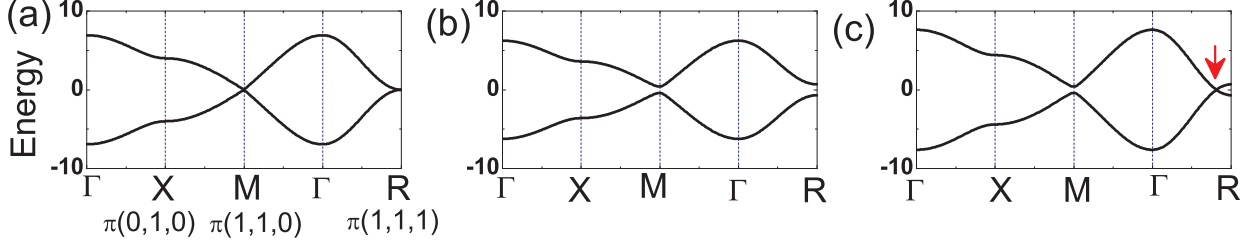


FIG. 2: Energy spectrum along high-symmetry lines in the first BZ for (a) $d=0$, (b) $d=0.2$, and (c) $d=-0.2$.

occurs. Following Ref. [16], we express the distortion along the $[1,1,1]$ direction by putting the transfer integral within the $(1,1,1)$ plane as $t_{\text{intra}}=1$, while that between the planes as $t_{\text{inter}}=1-d$. As the unit cell is cubic shown in Fig. 1, the first Brillouin zone (BZ) is cubic: $[-\frac{\pi}{a}, \frac{\pi}{a}]^3$. From now on, we set $a=1$. Then the Hamiltonian matrix $H_{\mathbf{k}}$ for each \mathbf{k} is given by

$$H_{\mathbf{k}} = \begin{pmatrix} 0 & e^{-i\frac{\pi}{6}} f_2 & e^{i\frac{\pi}{6}} f_1 & f_3 \\ e^{i\frac{\pi}{6}} f_2 & 0 & e^{-i\frac{\pi}{6}} f_3 & e^{i\frac{2\pi}{3}} f_1 \\ e^{-i\frac{\pi}{6}} f_1 & e^{i\frac{\pi}{6}} f_3 & 0 & e^{-i\frac{2\pi}{3}} f_2 \\ f_3 & e^{-i\frac{2\pi}{3}} f_1 & e^{i\frac{2\pi}{3}} f_2 & 0 \end{pmatrix}, \quad (16)$$

where $f_1=2(1-d)\cos(\frac{k_z+k_x}{2})+2\cos(-\frac{k_z+k_x}{2})$, $f_2=2(1-d)\cos(\frac{k_x+k_y}{2})+2\cos(-\frac{k_x+k_y}{2})$, $f_3=2(1-d)\cos(\frac{k_y+k_z}{2})+2\cos(-\frac{k_y+k_z}{2})$. In this Hamiltonian, the two lower bands are fully degenerate, $\varepsilon_{1\mathbf{k}}=\varepsilon_{2\mathbf{k}}(\mathbf{k})=-\sqrt{f_1^2+f_2^2+f_3^2}$, while the two upper bands are also degenerate with $\varepsilon_{3,4\mathbf{k}}=\sqrt{f_1^2+f_2^2+f_3^2}$. The band structure along high-symmetry lines in the first BZ is shown in Fig. 2. At $d=0$ [Fig. 2(a)], the upper and lower dispersions touch along the edge of the BZ and comprises an assembly of the massless Dirac fermions (Weyl fermions) in $(2+1)$ D. For $d>0$ (elongation along $[1,1,1]$ direction), all the Weyl fermions along the edge open a gap and turn into the massive Dirac fermions [Fig. 2(b)]. Therefore the gap fully opens in the density of states centered at zero energy. For $d<0$ (suppression along $[1,1,1]$ direction), all the $(2+1)$ D Weyl fermions along the edges open the gap as in the case of $d>0$. However, there occurs two additional $(3+1)$ D Weyl fermions [Fig. 2(c)] at $(k_x, k_y, k_z) = \pm D(1, 1, 1)$, where $D \equiv \arccos(\frac{1}{d-1})$ and \pm correspond to the right- and left-handed chirality [26]. Thus unlike $d>0$, the gap does not fully open in the case of $d<0$ due to the presence of a new single contact between the upper and lower bands in the BZ. The

normalized eigenvectors are given by

$$\begin{aligned}
|u_{1\mathbf{k}}\rangle &= \frac{1}{\sqrt{2}} \left(-\frac{f_1\varepsilon_{1\mathbf{k}}+if_2f_3}{\varepsilon_{1\mathbf{k}}\sqrt{f_1^2+f_2^2}}, e^{-i\frac{\pi}{3}}\frac{f_2\varepsilon_{1\mathbf{k}}-if_1f_3}{\varepsilon_{1\mathbf{k}}\sqrt{f_1^2+f_2^2}}, 0, -\frac{\sqrt{f_1^2+f_2^2}}{\varepsilon_{1\mathbf{k}}} \right)^\top, \\
|u_{2\mathbf{k}}\rangle &= \frac{1}{\sqrt{2}} \left(e^{i\frac{\pi}{6}}\frac{f_2}{\varepsilon_{2\mathbf{k}}}, e^{-i\frac{\pi}{6}}\frac{f_1}{\varepsilon_{2\mathbf{k}}}, 1, ie^{i\frac{\pi}{6}}\frac{f_3}{\varepsilon_{2\mathbf{k}}} \right)^\top, \\
|u_{3\mathbf{k}}\rangle &= \frac{1}{\sqrt{2}} \left(\frac{f_1\varepsilon_{3\mathbf{k}}+if_2f_3}{\varepsilon_{3\mathbf{k}}\sqrt{f_1^2+f_2^2}}, -e^{-i\frac{\pi}{3}}\frac{f_2\varepsilon_{3\mathbf{k}}-if_3f_1}{\varepsilon_{3\mathbf{k}}\sqrt{f_1^2+f_2^2}}, 0, \frac{\sqrt{f_1^2+f_2^2}}{\varepsilon_{3\mathbf{k}}} \right)^\top, \\
|u_{4\mathbf{k}}\rangle &= \frac{1}{\sqrt{2}} \left(e^{i\frac{\pi}{6}}\frac{f_2}{\varepsilon_{4\mathbf{k}}}, e^{-i\frac{\pi}{6}}\frac{f_1}{\varepsilon_{4\mathbf{k}}}, 1, ie^{i\frac{\pi}{6}}\frac{f_3}{\varepsilon_{4\mathbf{k}}} \right)^\top.
\end{aligned} \tag{17}$$

The Berry curvatures for these four Bloch bands are derived to have the form

$$\Omega_n^\alpha(\mathbf{k}) = \frac{F_{\beta\gamma}}{2\varepsilon_{n\mathbf{k}}^3} \tag{18}$$

with

$$F_{\beta\gamma} = f_1\frac{\partial f_2}{\partial k_\beta}\frac{\partial f_3}{\partial k_\gamma} + f_3\frac{\partial f_1}{\partial k_\beta}\frac{\partial f_2}{\partial k_\gamma} - f_2\frac{\partial f_1}{\partial k_\beta}\frac{\partial f_3}{\partial k_\gamma}, \tag{19}$$

where (α, β, γ) represent a cyclic permutation of (x, y, z) .

Let us see the Hall conductivity of this system [16] with $d \neq 0$. In the integer filling case, the zero-temperature Hall conductivity is a sum of Chern invariant [27] over occupied Bloch bands,

$$\sigma_{xy} = (e^2/h) \sum_n^{\text{occu}} \int_{[-\pi:\pi]} \frac{dk_z}{2\pi} C_n(k_z), \tag{20}$$

where the 2D Chern number [28] $C_n(k_z)$ is given by

$$\begin{aligned}
C_n(k_z) &= -\frac{1}{2\pi} \int_{[-\pi:\pi]^2} dk_x dk_y \Omega_n^z(\mathbf{k}) \\
&= -\frac{1}{2\pi} \int_{[-\pi:\pi]^2} dk_x dk_y \hat{z} \cdot (\nabla_{\mathbf{k}} \times \mathbf{A}_n(\mathbf{k})).
\end{aligned} \tag{21}$$

Here $\mathbf{A}_n(\mathbf{k})=i\langle u_{n\mathbf{k}}|\nabla_{\mathbf{k}}u_{n\mathbf{k}}\rangle$ is the Berry phase connection (vector potential) for n -th band. To proceed one may first transform the integral of $\nabla_{\mathbf{k}} \times \mathbf{A}_n$ over the first BZ to the line integral of \mathbf{A}_n along the BZ boundary by use of Stokes' theorem, and then apply the complex contour integration technique and residue theorem to sinusoidal functions. After a straightforward derivation, one obtains the non-zero Chern number, $C_1(k_z) = -\text{sgn}(g(k_z))$, $C_3 = \text{sgn}(g(k_z))$, where

$$g(k_z) = 2 + 2(1-d)\cos(k_z + 2k_P) \tag{22}$$

and $k_P = \arctan \left[\frac{(d-1)\cos k_z - 1}{(d-1)\sin k_z} \right]$. It is easy to verify that for $d>0$, the value of $g(k_z)$ is always positive, independent of k_z . For $d<0$, the sign of $g(k_z)$ depends on k_z in such a way that

$g(k_z) < 0$ for $k_z \in (-D, D)$ and $g(k_z) > 0$ for $k_z \in [-\pi, -D) \cup (D, \pi]$. Note that the present choice of the other two Bloch states $|u_{2\mathbf{k}}\rangle$ and $|u_{4\mathbf{k}}\rangle$ makes them to have no contribution to the Chern number.

However, the above purely mathematical calculation of 2D Chern number is not favored by theoretical physicists, who would like to resort to the physical connotation that the vector potential \mathbf{A}_n and gauge flux Ω_n are endowed with. Correspondingly, here we present this gauge-field analysis of the lower band $\varepsilon_{1\mathbf{k}}$ as an example. The value of 2D Chern number $C_1(k_z)$, which is confined to the (k_x, k_y) subspace at fixed k_z , is invariant under gauge transformation $|u'_{1\mathbf{k}}\rangle = e^{i\varphi_1(\mathbf{k})}|u_{1\mathbf{k}}\rangle$, $\mathbf{A}'_1(\mathbf{k}) = \mathbf{A}_1(\mathbf{k}) - \nabla_{\mathbf{k}}\varphi_1(\mathbf{k})$, where $\varphi_1(\mathbf{k})$ is an arbitrary smooth function of \mathbf{k} . If the gauge choice for $|u_{1\mathbf{k}}\rangle$ is well-defined everywhere in the whole (k_x, k_y) subspace in the first BZ, then its Chern number $C_1(k_z)$ will obviously be zero. However, at point $\mathbf{k}_0 = (k_z + 2k_P, k_z, k_z)$, one can find that the wave function $|u_{1\mathbf{k}}\rangle$ in Eq. (17) is ill-defined since both its denominator and numerator are zero at this point. This means that the used gauge cannot apply to the whole BZ and one needs to render a gauge transformation to avoid the singularity at \mathbf{k}_0 . For this one transforms the wave function to

$$|u'_{1\mathbf{k}}\rangle = \frac{1}{\sqrt{2}} \left(-\frac{f_2\varepsilon_{1\mathbf{k}} + if_1f_3}{\varepsilon_{1\mathbf{k}}\sqrt{f_2^2 + f_3^2}}, e^{-i\frac{\pi}{3}} \frac{f_3\varepsilon_{1\mathbf{k}} - if_1f_2}{\varepsilon_{1\mathbf{k}}\sqrt{f_2^2 + f_3^2}}, 0, -\frac{\sqrt{f_2^2 + f_3^2}}{\varepsilon_{1\mathbf{k}}} \right)^T. \quad (23)$$

The new eigenvector $|u'_{1\mathbf{k}}\rangle$ recovers the well-defined behavior at \mathbf{k}_0 ; the new singularity brought about is at $\mathbf{k}'_0 = (k_z, k_z + 2k_P, k_z)$. Thus according to the two different gauge choices, the BZ cross section at fixed k_z is now divided into two regions V and V' as shown in Fig. 3 ($k_z=0$). The wave functions $|u_{1\mathbf{k}}\rangle$ are used onto the region V, while $|u'_{1\mathbf{k}}\rangle$ apply to V'. Note that there remains some freedom in the division of the BZ. Because $|u_{1\mathbf{k}}\rangle$ and $|u'_{1\mathbf{k}}\rangle$ are ill-defined only at \mathbf{k}_0 and \mathbf{k}'_0 , respectively, we are free to deform this division as long as $\mathbf{k}_0(\mathbf{k}'_0) \notin V(V')$. This corresponds to the gauge degree of freedom [29, 30]. At $\mathbf{k} \in V \cap V'$, the two choices of wave functions are different by a phase factor $|u'_{1\mathbf{k}}\rangle = e^{i\varphi_1(\mathbf{k})}|u_{1\mathbf{k}}\rangle$, i.e., $\mathbf{A}'_1(\mathbf{k}) = \mathbf{A}_1(\mathbf{k}) - \nabla_{\mathbf{k}}\varphi_1(\mathbf{k})$, where

$$e^{i\varphi_1(\mathbf{k})} = \sqrt{\frac{f_2^2 + f_1^2}{f_3^2 + f_2^2} \frac{f_2\varepsilon_{1\mathbf{k}} + if_3f_1}{f_1\varepsilon_{1\mathbf{k}} + if_2f_3}}. \quad (24)$$

Thus one obtains the value of nonzero 2D Chern number for lower band $\varepsilon_1(\mathbf{k})$ as follows

$$\begin{aligned} C_1(k_z) &= -\frac{1}{2\pi} \oint_{\partial V} [\mathbf{A}_1(\mathbf{k}) - \mathbf{A}'_1(\mathbf{k})] \cdot d\mathbf{k} \\ &= -\frac{1}{2\pi} \oint_{\partial V} d\varphi_1(\mathbf{k}) = -\text{sgn}(g(k_z)), \end{aligned} \quad (25)$$

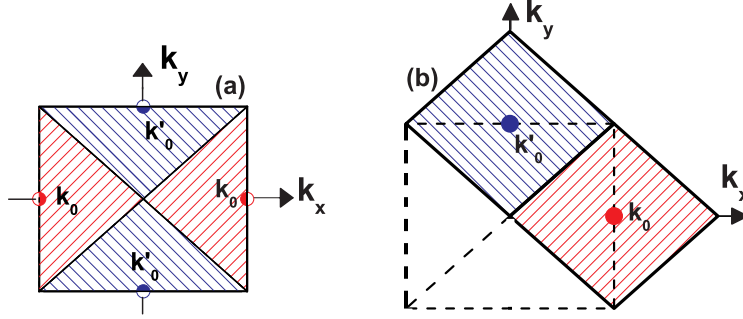


FIG. 3: (Color online). Division of cross section ($k_z=0$) of the first BZ into two regions V (red area) and V' (blue area). Note that the projection of the singularities \mathbf{k}_0 and \mathbf{k}'_0 onto (k_x, k_y) subspace vary with k_z .

which is consistent with the explicit calculation based on the complex-contour integration technique.

Consider the $\mu=0$ case, i.e., the two lower degenerate bands are fully filled while the two upper degenerate bands are empty. Then a further k_z -integral of $C_1(k_z)$ gives the Hall conductivity $\sigma_{xy} = -\frac{e^2}{h}$ for $d>0$ and $\sigma_{xy} = \frac{e^2}{h} \left(\frac{2D}{\pi} - 1\right)$ for $d<0$. The asymmetry of σ_{xy} between $d>0$ and $d<0$ will be explained below together with the behavior of the OM. When the local spins $\{\vec{S}_i\}$ are inverted (which means that the spin chirality is also inverted), then the Hall conductivity changes its sign.

IV. ORBITAL MAGNETIZATION AND ITS EFFECTS

Now we turn to study the OM and its various effects. Without loss of generality, the present attention is only on the z -component of the OM which is connected with Hall conductivity σ_{xy} . First, after a straightforward derivation, one obtains the k -space orbital magnetic moment as follows

$$m_n^z(\mathbf{k}) = \frac{F_{xy}}{2\varepsilon_n^2(\mathbf{k})}. \quad (26)$$

See Eq. (19) for F_{xy} . One can see that the orbital magnetic moment is identical for upper and lower bands, while the Berry curvatures [Eq. (18)] for upper and lower bands differ by a sign. A comparison between Eq. (26) and Eq. (18) gives an interesting relation for the present model

$$m_n^z(\mathbf{k}) = \Omega_n^z(\mathbf{k})\varepsilon_{n\mathbf{k}}. \quad (27)$$

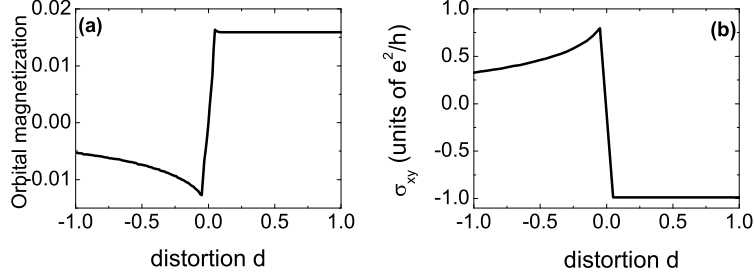


FIG. 4: (a) Zero-temperature orbital magnetization \mathcal{M}_z and (b) Hall conductivity σ_{xy} as a function of distortion d . The Fermi energy in (a) is chosen to be $\mu_0=0.1$, while in (b) the Fermi energy is chosen to be $\mu_0=0.0$ which corresponds to case that only the lower bands are fully occupied.

Given the expressions for $m_n^z(\mathbf{k})$ and $\Omega_n^z(\mathbf{k})$, the OM \mathcal{M}^z can now be systematically studied. At zero temperature, in particular, by substituting Eq. (27) into Eq. (4) one finds an important relation

$$\begin{aligned} \mathcal{M}_z &= \frac{e}{\hbar} \mu_0 \sum_n \int^{\mu_0} d^3\mathbf{k} \Omega_n^z(\mathbf{k}) \\ &= -\frac{\mu_0}{e} \sigma_{xy}, \end{aligned} \quad (28)$$

which indicates that the OM is proportional to the Hall conductivity with coefficient $(-\mu_0/e)$. Equation (28) also holds at low temperature. Although this remarkable relation between the OM and the Hall conductivity is specific to the present Hamiltonian model, it definitely tells one that the topological ingredient in the OM may be faithfully mapped out through the Hall conductivity. If the band is partially filled, then after integrating by parts one finds that Eq. (28) can be written as a pure Fermi-surface integral. In the integer filling case, on the other hand, the OM and Hall conductivity display a Fermi-sea feature. Figure 4 shows \mathcal{M}_z and σ_{xy} as a function of the distortion d . The $d>0$ and $d<0$ cases are asymmetric by the observation that σ_{xy} is quantized for $d>0$ while non-quantized for $d<0$. To understand this asymmetry one may treat the distortion d as a control parameter of the 3D band structure and start from $d=0$, at which the upper and lower bands are degenerate along the BZ edge, i.e., $(k_x=\pm\pi, k_y=\pm\pi, k_z)$, $(k_x=, k_y=\pm\pi, k_z=\pm\pi)$, $(k_x=\pm\pi, k_y, k_z=\pm\pi)$. When d is varied from $d=0$ to $d>0$, then these initial degenerate points *completely* split into two groups of “Dirac point” singularities, which play the role of positive and negative monopole sources, respectively [see, as an example, \mathbf{k}_0 and \mathbf{k}'_0 points in Fig. 2]. The upper and lower

bands are now tightly coupled by a series of “Berry flux loops”. Along each loop Berry curvature flux 2π passes from the lower bands to the upper bands through one Dirac point, then returns through the other corresponding one. The positive (negative) monopoles of the lower bands and the negative (positive) monopoles of the upper bands may recombine by a relative displacement of a primitive reciprocal lattice vector \mathbf{G} . In the present cubic lattice the \mathbf{G} is along one selective \hat{k}_α -axis ($\alpha = x, y, z$) with amplitude 2π (the lattice constant a has been scaled to be unity). This means that during the “Dirac point” splitting process, the individual Chern invariant (the 3D generalization of 2D Chern number) for the lower and upper bands changes by $\mp\mathbf{G}$, respectively, while their sum is conserved. As a result, the Hall conductivity σ_{xy} for lower/upper bands is quantized to be a product of $\frac{e^2}{h}$ and the following Chern invariant

$$\frac{1}{2\pi} \int_{[-\pi:\pi]^3} d^3\mathbf{k} \Omega_n^z(\mathbf{k}) = -\frac{1}{2\pi} C_n G_z. \quad (29)$$

When d is varied from $d=0$ to $d<0$, equation (29) breaks down, since the 2D Chern number C_n is now k -dependent by the presence of the additional two (3+1)D Weyl fermions at $(k_x, k_y, k_z) = \pm D(1, 1, 1)$. In this case, although the gap is opened at Dirac points along the BZ edge, the emergence of new Weyl fermions contributes non-zero density of states in the gap. It is then straightforward to repeat the integration in Eq. (29) by parts to expose the non-quantized part of the 3D intrinsic Hall conductivity as a Fermi surface property.

In the half filled case, i.e., when the chemical potential is in the Mott gap, the Hall conductivity vanishes due to the cancellation of the Chern invariants of the upper and lower bands. As a consequence, the OM in Eq. (29) also vanishes. This result is prominently different from that in Ref. [16], in which a finite OM with amplitude smoothly varied with distortion d was given via a tight-binding calculation. Ref. [16] employed the Kubo-Streda formula in calculating the OM. As we have shown above, however, the Kubo-Streda formula and the semiclassical formula give the same expression for the intrinsic OM. So no discrepancy is expected to occur between the two approaches. The non-zero OM in Ref. [16] in the Mott gap was ascribed by the authors to be a bulk Fermi sea property. However, the present explicit relation Eq. (29) together with Haldane’s argument on the metallic AHE [11] shows that the non-quantized part of the OM in the present model is a Fermi-surface Berry phase effect, while the quantized part is completely determined by the topology of the filling bands.

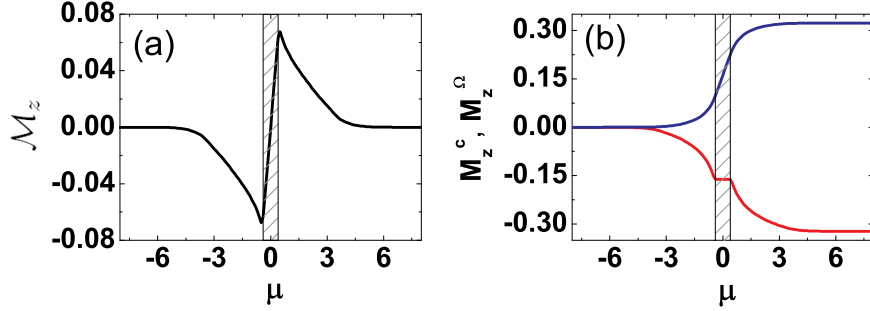


FIG. 5: (Color online). (a) Orbital magnetization \mathcal{M}_z , and (b) its two components M_c^z (red curve) and M_Ω^z (blue curve) as a function of the electron chemical potential μ for distortion $d=0.2$. The shaded area is the gap between the lower and upper bands. To suppress the divergence at band/gap contact, we have used the temperature of $k_B T=0.05$.

Figure 5(a) shows the \mathcal{M}_z as a function of the electron chemical potential μ for the distortion $d=0.2$. One can see that initially the OM rapidly decreases as the filling of the lower bands increases, arriving at a minimum at $\mu=-0.4$, a value corresponding to the top of the lower band. Then, as the chemical potential continues to vary in the gap [shaded region in Fig. 5(a)] between the lower and upper bands, the OM goes up and increases as a linear function of μ . This linear relationship in the insulating region is explicit from Eq. (28). When the chemical potential touches the bottom of the upper band, then the linear increase in \mathcal{M}_z suddenly stops and the OM rapidly decreases again by going the chemical potential through the upper bands. The turning behavior at the band/gap contacts becomes numerically divergent at $k_B T=0$. This discontinuity is due to the singular behavior of $\Omega_n(\mathbf{k})$ at the BZ edge point $\mathbf{k}=\mathbf{k}_0$, which will play its role when the k -integral is over the entire BZ.

The distinct behavior of the OM in the metallic and insulating regions, as shown in Fig. 5(a), reflects the different roles that its two components M_c^z and M_Ω^z play in these two regions. To see this, we show in Fig. 5(b) M_c^z (blue curve) and M_Ω^z (red curve) as a function of μ . One can see that M_c^z and M_Ω^z oppose each other, which implies that they are carried by opposite-circulating currents. Also one can see that in the band insulating regime, the conventional term M_c^z keeps a constant during variation of μ . This behavior is due to the fact that the upper limit of the k -integral of $\mathbf{m}_n(\mathbf{k})$ is invariant as the chemical potential varies in the band gap. In the metallic region, however, since the occupied states

varies with the chemical potential μ , thus \mathbf{M}_c also varies with μ , resulting in a decreasing slope shown in Fig. 5(b). The Berry phase term \mathbf{M}_Ω also displays different features in the insulating and metallic regions. In the insulating region, \mathbf{M}_Ω linearly increases with μ , as is expected from Eq. (28). In the metallic region, however, this term keeps a constant with the amplitude sensitively depending on the topological property of the band in which the chemical potential is located. On the whole it reveals in Fig. 3 that the metallic behavior of the OM is dominated by its conventional term \mathbf{M}_c , while in the insulating regime the Berry phase term \mathbf{M}_Ω comes to play a main role in determining the behavior of the OM.

The above separate discussion of \mathbf{M}_c and \mathbf{M}_Ω can be transferred to study the anomalous Nernst effect (ANE). The relation between the OM and ANE has been recently found [3]. To discuss the transport measurement, it is important to discount the contribution from the magnetization current, a point which has attracted much discussion in the past. Cooper et al. [31] have argued that the magnetization current cannot be measured by conventional transport experiments. Xiao et al. [3] have adopted this point and built up a remarkable picture that the conventional orbital magnetic moment \mathbf{M}_c does not contribute to the transport current, while the Berry phase term in Eq. (3) directly enters and therefore modifies the intrinsic Hall current as follows

$$\mathbf{j}_H = -\frac{e^2}{\hbar} \mathbf{E} \times \sum_n \int \frac{d^3k}{(2\pi)^3} f_n(\mathbf{r}, \mathbf{k}) \Omega_n(\mathbf{k}) - \nabla \times \mathbf{M}_\Omega(\mathbf{r}), \quad (30)$$

In the case of uniform temperature and chemical potential, obviously, the second term is zero and the Hall effect of the distorted fcc lattice is featured by the first term in Eq. (30). In the following, however, we turn to study another situation, where the driving force is not provided by the electric field. Instead, it is provided by a statistical force, i.e., the gradient of temperature T . In this case, Eqs. (30) and (3) give the expression of intrinsic thermoelectric Hall current as $j_x = \alpha_{xy}(-\nabla_y T)$, where the anomalous Nernst conductivity α_{xy} is given by

$$\begin{aligned} \alpha_{xy} = & \frac{1}{T} \frac{e}{\hbar} \sum_n \int \frac{d^3k}{(2\pi)^3} \Omega_n \\ & \times [(\epsilon_{n\mathbf{k}} - \mu) f_n + k_B T \ln(1 + e^{-\beta(\epsilon_{n\mathbf{k}} - \mu)})]. \end{aligned} \quad (31)$$

Figure 6 shows α_{xy} of the distorted fcc lattice as a function of the chemical potential for $d = 0.2$ and $k_B T = 0.05$. One can see that the ANE disappears in the insulating regions, and when scanning μ through the contacts between the bands and gaps, there will appear

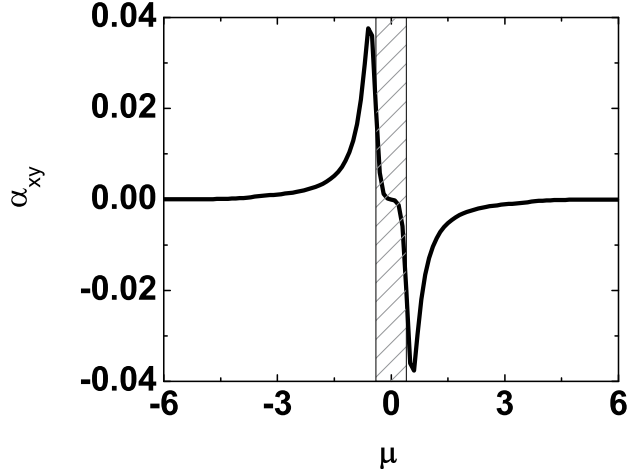


FIG. 6: The intrinsic anomalous Nernst conductivity α_{xy} as a function of the electron chemical potential μ for $d=0.2$ and $k_B T=0.05$. The shaded area is the gap between the lower and upper bands.

peaks and valleys. Remarkably, a similar peak-valley structure was also found by the recent first-principles calculations in CuCr_2Se_4 compound [3]. The ANE of this compound was recently measured by Lee et al. [6] as a function of Br doping which substitutes Se in the compound and changes the chemical potential μ . Due to the scarce data available, until now the peak-valley structure of α_{xy} revealed in Fig. 6 and in Ref. [3] has not been found in experiment, and more direct experimental results are needed for quantitative comparison with the theoretical results. Interestingly, the expression for α_{xy} can be simplified at low temperature as the Mott relation [3],

$$\alpha_{xy} = -\frac{\pi^2 k_B^2 T}{3} \frac{\partial \sigma_{xy}(\mu_0)}{\partial \mu_0}. \quad (32)$$

Thus one can see that the low-temperature nonzero ANE is a Fermi-surface Berry phase effect. Another unique feature of α_{xy} is its linear dependence of temperature.

V. CONCLUSION

In summary, after pointing out the equivalence of the semiclassical approach and the quantum Kubo-Streda formula in description of the intrinsic orbital magnetization, we have theoretically studied the properties of the OM in antiferromagnets on the distorted 3D fcc lattice. The distortion parameter d in the fcc lattice produces nonzero 2D Chern number

and results in profound effects on the OM properties. An explicit relation between the OM and the Hall conductivity in this system has been derived. According to this relation we have found that the OM vanishes when the electron chemical potential is lies in the Mott gap, which is in contrast with the results in Ref. [16]. We have shown that the two parts \mathbf{M}_c and \mathbf{M}_Ω in the OM oppose each other, and yield the paramagnetic and diamagnetic responses, respectively. In particular, due to its Fermi-sea topological property, the magnetic susceptibility of \mathbf{M}_Ω remains to be a nonzero constant when the Fermi energy is located in the energy gap. It has been further shown that the OM displays distinct behavior in the metallic and Chern-insulating regions, because of different roles \mathbf{M}_c and \mathbf{M}_Ω play in these two regions. The anomalous Nernst conductivity has been studied, which displays a peak-valley structure as a function of the electron chemical potential. We expect that these results will be experimentally verified in the spin-frustrated systems.

Acknowledgments

This work was supported by CNSF under Grant No. 10544004 and 10604010.

-
- [1] D. Xiao, J. Shi, and Q. Niu, Phys. Rev. Lett. **95**, 137204 (2005).
 - [2] T. Thonhauser, D. Ceresoli, D. Vanderbilt, and R. Resta, Phys. Rev. Lett. **95**, 137205 (2005).
 - [3] D. Xiao, Y. Yao, Z. Fang, and Q. Niu, Phys. Rev. Lett. **97**, 026603 (2006).
 - [4] M.-C. Chang and Q. Niu, Phys. Rev. B **53**, 7010 (1996).
 - [5] G. Sundaram and Q. Niu, Phys. Rev. B **59**, 14915 (1999).
 - [6] W.-L. Lee, S.Watauchi, V.L. Miller, R.J. Cava, and N.P. Ong, Science **303**, 1647 (2004); Phys. Rev. Lett. **93**, 226601 (2006).
 - [7] D. Ceresoli, T. Thonhauser, D. Vanderbilt, and R. Resta, Phys. Rev. B **74**, 024408 (2006).
 - [8] Z. Wang and P. Zhang, e-print, cond-mat/0704.3305v1
 - [9] F.D.M. Haldane, Phys. Rev. Lett. **61**, 2015 (1988).
 - [10] K. Ohgushi, S. Murakami, and N. Nagaosa, Phys. Rev. B **62**, R6065 (2000).
 - [11] F.D.M. Haldane, Phys. Rev. Lett. **93**, 206602 (2004).
 - [12] P. Streda, J. Phys. C: Solid State Phys., **15**, L717 (1982).

- [13] D.J. Thouless, M. Kohmoto, M.P. Nightgale, and M. den Nijs, Phys. Rev. Lett. **49**, 405 (1982).
- [14] K. Wakabayashi, M. Fujita, H. Ajiki, and M. Sigrist, Phys. Rev. B **59**, 8271 (1999).
- [15] P. Streda, J. Kucera, D. Pfannkuche, R.R. Gerhardtts, and A.H. MacDonald, Phys. Rev. B **50**, 11955 (1994).
- [16] R. Shindou and N. Nagaosa, Phys. Rev. Lett. **87**, 116801 (2001).
- [17] A. Sakuma, J. Phys. Soc. Jpn. **69**, 3072 (2000).
- [18] J.A. Wilson and G.D. Pitt, Philos. Mag. **23**, 1297 (1971); K. Kikuchi et al., J. Phys. Soc. Jpn. **45**, 444 (1978).
- [19] Y. Endoh and Y. Ishikawa, J. Phys. Soc. Jpn. **30**, 1614 (1971).
- [20] T. Thio, J.W. Benett, and T.R. Thurston, Phys. Rev. B **52**, 3555 (1995).
- [21] T. Thio and J.W. Benett, Phys. Rev. B **50**, 10574 (1994).
- [22] K. Adachi, M. Matsui, and Y. Omata, J. Phys. Soc. Jpn. **50**, 83 (1981).
- [23] K. Yoshida and S. Inagaki, J. Phys. Soc. Jpn. **50**, 3268 (1980).
- [24] A. Yoshimori and S. Inagaki, J. Phys. Soc. Jpn. **50**, 769 (1981).
- [25] V. Kalmeyer and R. B. Laughlin, Phys. Rev. Lett. **59**, 2095 (1987); G. Baskaran and P. W. Anderson, Phys. Rev. B **37**, 580 (1988); R. B. Laughlin, Science **242**, 525 (1988); X. G. Wen, F. Wilczek, and A. Zee, Phys. Rev. B **39**, 11413 (1989).
- [26] H.B. Nielsen and M. Ninomiya, Phys. Lett. B **130**, 389 (1983).
- [27] M. Kohmoto, B.I. Halperin, and Y.-S. Wu, Phys. Rev. B **45**, 13488 (1992).
- [28] D.J. Thouless, *Topological Quantum Numbers in Nonrelativistic Physics* (World Scientific, Singapore, 1998).
- [29] M. Kohmoto, Ann. Phys. (N.Y.) **160**, 343 (1985).
- [30] S. Murakami and N. Nagaosa, Phys. Rev. Lett. **90**, 057002 (2003).
- [31] N.R. Cooper, B.I. Halperin, and I.M. Ruzin, Phys. Rev. B **55**, 2344 (1997).